A lateral boundary formulation for multi-level prediction models

By H. C. DAVIES*

NASA-Langley Research Center, Hampton, VA 23665

SUMMARY

An expedient method is proposed for the lateral boundary treatment of a limited-area prediction model. The method involves the relaxation of the interior flow in the vicinity of the boundary to the external fully prescribed flow. A systematic study of the method is undertaken with an (x, z), linear, primitive equation model. Analytical considerations of the method for the continuous equations demonstrate the manner in which the method consumes gravity wave energy, error and fine spatial scale potential vorticity near the lateral boundaries. Numerical experiments are also undertaken to assess the usefulness of the method. The results indicate that the method gives an adequate representation of outgoing gravity waves with and without an ambient shear flow, and also allows the substantially undistorted transmission of geostrophically balanced flow out of the interior of the limited domain.

On the basis of these results, it is suggested that the method constitutes a promising utilitarian treatment of the lateral boundaries.

1. INTRODUCTION

Lateral boundaries invariably form an intrinsic feature of numerical weather prediction models, since perforce almost all models are not global in extent. Difficulties associated with the treatment of these boundaries are partially circumvented in short-term integrations of comparatively coarse grid-point models of planetary and synoptic scale motion. This is achieved by taking the region of integration to be much larger than the particular region of interest or by assuming a slip-free boundary at the equator. A somewhat subtler lateral boundary problem is posed by regional forecast models. These models require a fine grid-point mesh to achieve the necessary resolution of the relevant sub-synoptic scale phenomena, but the use of the fine mesh is usually restricted, by severe operational, computational or physical constraints, to a limited region of the complete flow domain. It then follows that time dependent boundary conditions are required to close formally the initial boundary value problem posed by a limited-area prediction model.

Two approaches have been adopted for supplying boundary data to the limited-area models. In one, the boundary data is specified externally with data from an integration performed with a coarser grid and larger domain (e.g. Williamson and Browning 1974; Chen and Miyakoda 1974). For the second approach, the fine-mesh model is dynamically coupled to the coarse-mesh model to form a single dynamic system (e.g. Harrison and Elsberry 1972; Price and MacPherson 1973). Phillips and Shukla (1973) referred to these two methods as the 'one-way' and 'two-way' interaction methods corresponding to the class of interactions permissible between the limited-region flow and the exterior flow.

In this paper our principal concern will be with the one-way interaction problem, and it appears to us imperative to recognize that in all practical applications, the available boundary data will inevitably contain inherent errors. Data derived from an integration with a coarser grid over a larger domain will contain characteristic features intrinsic to that model, and these features will differ from both the development of the atmosphere and the fields derived from the finer-mesh regional model. Features in this category include numerical effects such as those that lead to phase speed errors, and pseudo-physical effects

* Present affiliation: Department of Geophysics, University of Reading, Reading

such as parameterization schemes. A particular manifestation of these effects will be the development in the regional model of both gravity waves and balanced meteorological flow on a scale unresolved by the coarse mesh. These effects will render the boundary data incompatible with the flow of the regional model.

Thus it is evident that a lateral boundary treatment should serve a two-fold purpose. It should be capable of transmitting smoothly into and out of the limited domain the large-scale flow resolved by, and implicit in, the external boundary data. It should also adequately represent the outgoing gravity waves and fine-mesh-scale meteorological flow inherent in the initial data for the limited domain or generated *in situ* during the time integration.

Previous lateral boundary treatments for the one-way integration problem have taken two disparate forms. In the first approach, pragmatic techniques were employed to reduce lateral boundary noise. These include the insertion of a highly diffusive layer contiguous to the boundary (Benwell *et al.* 1971); the use of a 'divergence-control' method near the boundary of the limited domain to match the interior flow with boundary data derived from a coarser mesh geostrophic model (Okamura 1975); and the modification of the model tendencies near the boundary to induce a smooth transition from model tendencies in the interior to the tendencies of the external data at the boundary (Kesel and Winninghoff 1972; Perkey and Kreitzberg 1975).

In the second approach, one seeks to satisfy uniqueness and well-posedness criteria for the flow in the limited domain. Hence only boundary data corresponding to the transfer of information into the domain is specified at the boundary, i.e. only a subset of the dependent variables should be specified at the boundary. The problems associated with this approach are further compounded by the discretization schemes employed in numerical models because the difference equations will usually demand additional purely computational boundary conditions. Consideration of this approach has been given by Charney (1962) and recently by Kadyshnikov (1973), Davies (1973 a, b), Elvius and Sundström (1973), Chen and Miyakoda (1974), and Pearson (1974).

It is important to note that the complications associated with this second approach accrue from seeking an analytically justifiable coupling between the boundary data and the interior flow for the unmodified system of meteorological governing equations. Moreover, in the attendant theory it is presupposed that the required boundary data are free of error.

In the light of the preceding discussion, it appears desirable to seek an utilitarian boundary formulation that is consonant with the dynamical constraints of the governing equations but also alleviates the effect of the inaccurate boundary data. In this paper we present one such simple lateral boundary scheme. We systematically adulterate the governing equations to reduce their sensitivity to overspecification of boundary data, and in so doing, a reduction is also achieved in the noise generation at the lateral boundaries.

2. THE BOUNDARY FORMULATION

(a) Outline

We outline the lateral-boundary treatment in the context of a linear, primitive equation system. The system considered can sustain internal and external gravity waves and an advecting meteorological wave. Moreover, with a linearized system we can readily interpret the role of the boundary treatment.

We consider linearized, inviscid, compressible flow confined between two horizontal walls located at $z = 0, D$ on an f-plane. The flow is assumed independent of one horizontal co-ordinate (say y) with an unidirectional basic flow $U = U(z)$ that is in geostrophic balance

with an external force E ($E = fU$). The basic thermodynamic state is isothermal so that $\partial p_0/\partial z = \rho_0 g$, with $c^2 = \gamma p_0/\rho_0 = \gamma RT_0 =$ constant; and hence $S = \partial(\ln \theta_0)/\partial z =$ constant. Here we have employed conventional thermodynamic nomenclature.

It follows that the governing equations for the perturbation variables of our system take the following form (see Ogura and Charney 1962),

$$u_t + Uu_x + wU_z - fv = -p_x - K(u - \tilde{u}) \qquad . \qquad . \qquad . \qquad (1)$$

$$v_t + Uv_x + f(u + U) = E - K(v - \tilde{v}) + F[v - \tilde{v}] \qquad . \qquad . \qquad (2)$$

$$p_t + Up_x + c^2 u_x = -c^2(w_z + wS) - K(p - \tilde{p}) \qquad . \qquad . \qquad (3)$$

with a diagnostic equation for the vertical velocity, w,

$$w_{zz} + (S + g/c^2)w_z = -u_{xz} - (g/c^2)u_x - (U_z/c^2)p_x \qquad . \qquad (4)$$

where $(u, v, w) = \rho_0(u', v', w')$, the momentum components corresponding to the respective velocity components (u', v', w').

The mathematical formulation of the boundary treatment is contained in the terms involving the function K and the functional F in these equations. An estimate of the time development of the flow field in the neighbourhood of the boundary is assumed available for the time period of interest. This estimate is denoted by the overbarred fields $(\tilde{u}, \tilde{v}, \tilde{p})$. The specified function $K = K(x) \geqslant 0$ is continuous and non-zero only in the vicinity of the boundary. The functional F is defined by $F[v - \tilde{v}] = \int_{L^*}^{x} K_x(v - \tilde{v})\,dx$. The integral is evaluated from the point L* in the interior region to the required point. We note that the integral is non-zero only in the boundary region $K_x \neq 0$.

These terms act to constrain the prognostic variables in the neighbourhood of the boundaries toward the external fully prescribed fields. They can be interpreted as a dynamical relaxation, reminiscent of a 'Newtonian law' adjustment of the normal velocity, pressure and potential vorticity fields about the external prescribed fields of those variables. The spatial dependency of the relaxation coefficient, K, contributes to the smooth transition from the interior flow field values to those of the field implied by the external data. We note that the relaxation coefficient is not a function of the vertical co-ordinate, and, hence, the diagnostic vertical velocity equation is unchanged by the lateral boundary treatment.

(b) Analysis

We now elaborate the rationale behind this somewhat obscure formulation. It is simpler to consider separately the two cases of purely irrotational flow and the advection of potential vorticity.

For the former case, we set identically zero the tangential velocity, the Coriolis parameter and the externally specified control field (i.e. $v \equiv f \equiv 0$, and $\tilde{u} \equiv \tilde{v} \equiv \tilde{p} \equiv 0$). Further, we assume the basic mean flow is constant. Subject to these restrictions, Eqs. (1)–(4) can then be rearranged to the form

$$u_t + Uu_x = -p_x - Ku, \qquad . \qquad . \qquad . \qquad (5)$$

$$(\mathscr{D}p)_t + U(\mathscr{D}p)_x = (gS)u_x - K(\mathscr{D}p), \qquad . \qquad . \qquad (6)$$

where $\mathscr{D}p = p_{zz} + (S + g/c^2)p_z$. The dependent variables u and p can be expanded into the appropriate vertical eigenfunctions, whereupon the equations for each vertical eigenmode corresponding to the external and internal gravity waves can assume the form

$$(u_i' \pm p_i)_t + (U \pm c_i)(u_i' \pm p_i)_x = -K(u_i' \pm p_i), \qquad . \qquad . \qquad (7)$$

where $c_i = c$ (sound speed) for the external mode,
and $c_i^2 = gS/\lambda_i^2,\ i = 1, 2, \ldots$ for internal modes
with $\mathscr{D}p = -\Sigma \lambda_i^2 p_i$ and $u_i' = c_i u_i$.

Here the subscript i refers to the eigenfunction expansions, whilst the remaining subscripts denote as before the space and time derivatives.

Eq. (7) is in pseudo-characteristic form. The quantities $(u_i' \pm p_i)$ are conserved along the velocity paths $x_t = U \pm c_i$ in the non-relaxed regions $(K = 0)$, and suffer a reduction in amplitude elsewhere. A quantitative measure of the amplitude reduction can be obtained as follows. Consider the decay of a scalar quantity ϕ, advecting with a velocity γ into a relaxation region.

The govering equation is

$$\phi_t + \gamma\phi_x = -K\phi, \qquad \qquad \qquad (8)$$

and let $K = 0$ for $0 \leqslant x$ and $K = ax^2$ for $x > 0$; with $\phi = \phi_0$ at $x = 0$.

Then the total advective change of the pulse is given by

$$\phi = \phi_0/\exp\{(a/3\gamma)x^3\} \quad \text{for} \quad x \geqslant 0 \qquad \qquad (9)$$

Thus the scalar ϕ decays exponentially in the relaxation boundary region, with the 'relaxation' distance for an e^{-1} reduction in amplitude given by $x^* = \sqrt[3]{(3\gamma/a)}$. It is clear that the relaxation distance of the eigenmodes of Eq. (7) will be a function of their Doppler shifted phase speed. The external gravity wave suffers the least amplitude reduction for typical meteorological mean-flow speeds.

Let us now consider the advection of potential vorticity. We allow the tangential velocity, v, and the Coriolis parameter, f, to be non-zero, but again assume the mean flow is constant. An appropriate advection equation is obtained by eliminating u_x between Eq. (6) and the x-derivative of Eq. (2) to yield:

$$Q_t + uQ_x = -KQ, \qquad \qquad \qquad (10)$$

where $Q = v_x + (f/gS)\mathscr{D}p$. Thus we again have a first-order hyperbolic equation in pseudo-characteristic form. We can infer that the propagation of potential vorticity into a relaxation region will diminish the amplitude of that scalar quantity as given by Eq. (9). Here the appropriate group velocity is the advective velocity, U, and this implies that the amplitude reduction will be of the order of, or much larger than, that suffered by gravity waves.

The analysis indicates that for this linear system of equations, subject to the stipulated conditions, the relaxation boundary treatment guides the values of the prognostic variables toward those of the externally specified fields. This is achieved in such a way as to reduce the amplitude of outgoing potential vorticity and gravity waves that are perturbations from the externally specified control fields. The treatment reduces the sensitivity of the interior flow to the overspecification of the variables at the lateral boundaries. In this manner the treatment alleviates problems associated with the well-posedness criteria of the non-relaxed equations. These properties should have a concomitant effect in reducing 'noise' generation at the lateral boundaries.

It must be noted that the analysis did not include the effect of vertical shear of the mean flow horizontal wind, and nonlinear effects. Furthermore, the conclusions derived here for the continuous equations are not automatically applicable to the difference equations. We examine the latter question in the next section.

We note in passing that an analysis similar to that used here can be applied to the pragmatic techniques mentioned in the introduction. Modification of the tendencies as carried out by Kesel and Winninghoff (1972) merely reduces the phase speed of waves as they approach the boundary, and it is necessary to provide an additional mechanism to

prevent energy build-up and spurious numerical reflection at the boundary. This was demonstrated by Perkey and Kreitzberg (1975). However, the technique also introduces a spurious source term for potential vorticity in the boundary region and this can induce spurious and unacceptable reflection.

Again, the boundary technique of divergence damping has a beneficial effect upon small wavelength gravity waves, but it is not designed to treat fine-scale meteorological flow that develops during the integration. Similar conclusions are applicable to the technique of introducing highly diffusive regions contiguous to the lateral boundaries.

3. NUMERICAL EXPERIMENTS

(a) The model

A nine-level finite difference model is constructed for the system listed in Eqs. (1)–(4). The model variables are structured as shown in Fig. 1. Horizontal and vertical mesh lengths are set respectively at 60 km and 1·3 km and there are 63 grid points in the horizontal. The boundary relaxation coefficient is given a parabolic spatial dependency and decreases to zero at a distance of five grid lengths from the boundary.
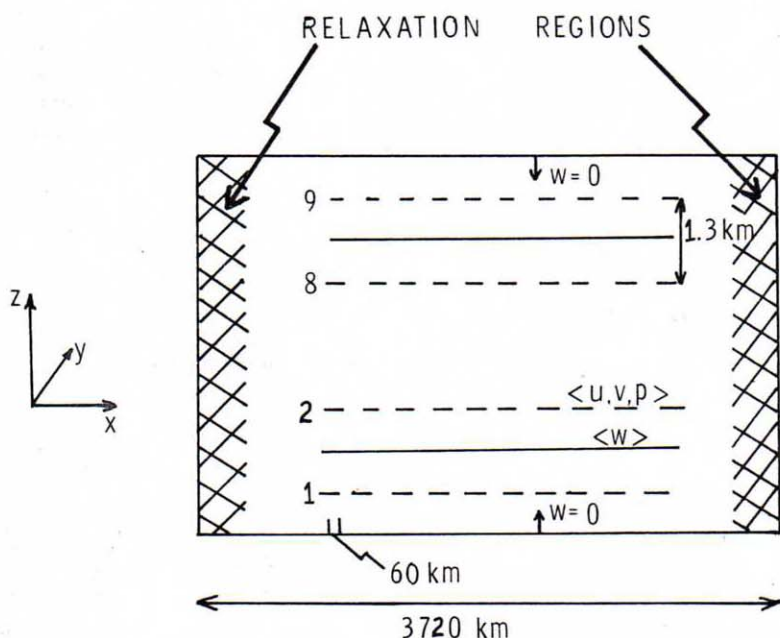

Figure 1. Schematic outline of the model's structure. Cross-hatched region denotes the boundary relaxation region ($K \neq 0$).

The difference scheme is second order, centred in space and time, except for the implicit treatment for the boundary terms. The difference analogue of Eq. (2) has the form

$$v_i^{n+1} = v_i^{n-1} - \alpha(v_{i+1}^n - v_{i-1}^n) - f(2\Delta t)u_i^n - K_i(2\Delta t)(v_i^{n+1} - \tilde{v}_i^{n+1}) +$$

$$+ (\Delta t) \sum_{j=1^*}^{i} (K_j - K_{j-1})(v_j^{n+1} - \tilde{v}_j^{n+1} + v_{j-1}^{n+1} - \tilde{v}_{j-1}^{n+1}) \ . \qquad \qquad (11)$$

where $\alpha = U\Delta t/\Delta x$, and the summation takes place from a point I* in the interior to the required point i.

Values assigned to the model parameters are as follows:
$c = 331\,\mathrm{m\,s^{-1}}; f = 1 \cdot 3 \times 10^{-4}\,\mathrm{s^{-1}}; S = 3 \cdot 58 \times 10^{-5}\,\mathrm{m^{-1}}; \Delta t = 120\,\mathrm{s}; K|_{\mathrm{bd}} = 4 \cdot 15 \times 10^{-3}\,\mathrm{s^{-1}}.$
For these values, we can infer from Eq. (9) that the amplitude reduction of even the external gravity wave is substantial in the boundary region (typically $\phi|_{\mathrm{bd}}/\phi_0 = 2 \times 10^{-2}$).

A series of numerical experiments were performed with this model to examine the behaviour of the boundary treatment under a variety of conditions.

(b) Treatment of gravity waves

The first set of experiments were designed to test the technique's treatment of outgoing gravity waves. For these experiments, the Coriolis parameter and the externally specified boundary field were set to zero. The initial conditions represented an isolated pressure pulse with a vertical structure corresponding to a single eigenmode of the shear-free system, and the model atmosphere was assumed to be initially at rest ($u = 0$) everywhere. Thus we
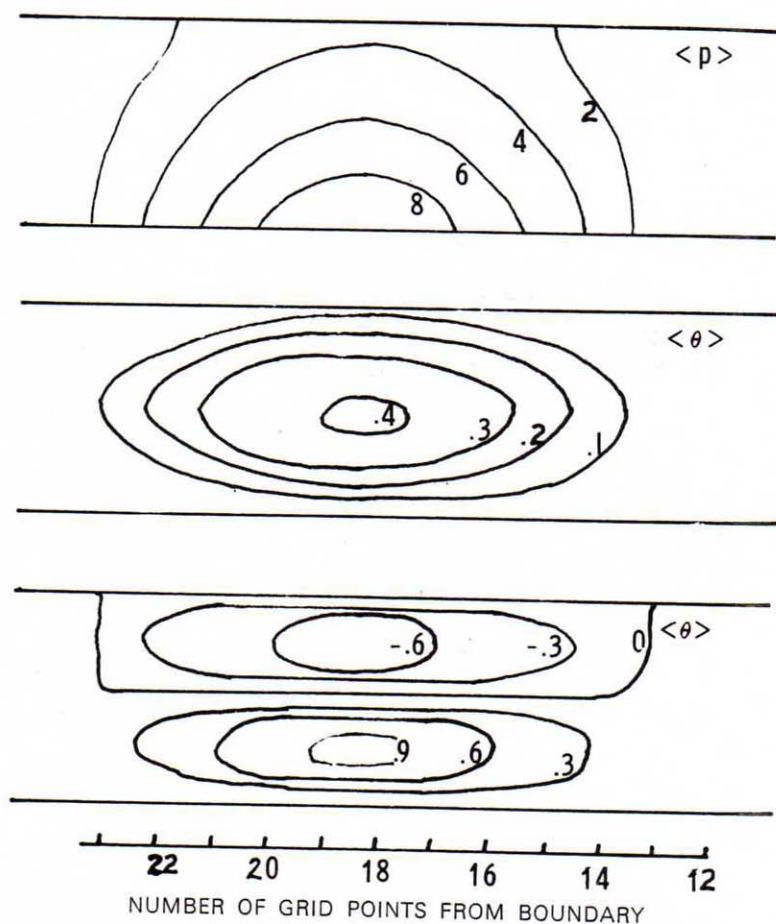

Figure 2.   Initial perturbations for the experiments on outgoing gravity waves. The pressure perturbation of the external mode is shown in mb, and the potential temperature perturbation of the first and second internal modes is displayed in K.

anticipate eastward and westward propagating pulses in the subsequent development. Three initial states were considered, corresponding to the external gravity mode, and the
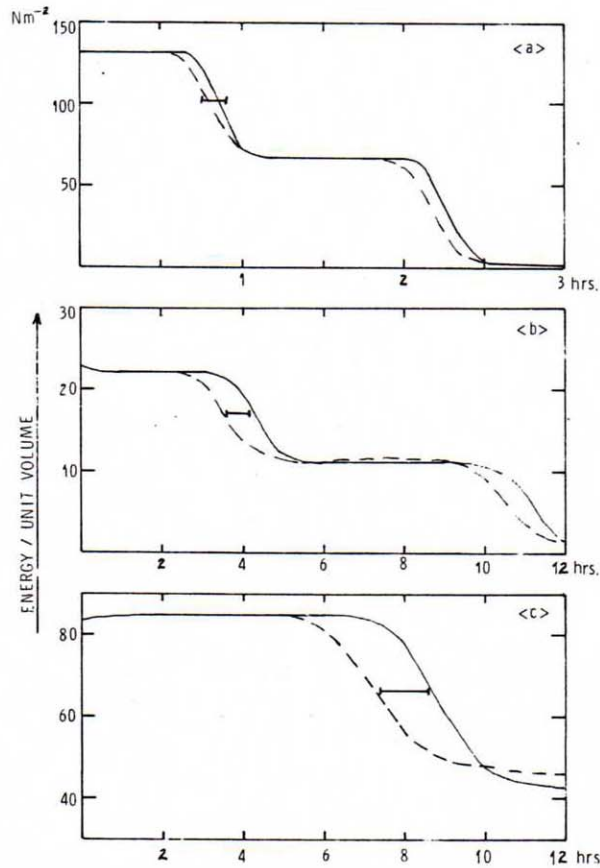
Figure 3.   Time variation of the total perturbation energy per unit volume for:— (a) the external mode, (b) the first internal mode, (c) the second internal mode in case of no shear. Dashed and solid lines correspond respectively to results with the limited domain with boundary relaxation, and the extended domain. Horizontal bar denotes time for mode to traverse the boundary region.

first and second internal modes. Fig. 2 depicts the perturbation pressure of the external mode and the perturbation potential temperature distribution of the internal modes. Analytical expressions for the vertical dependency of these modes have the forms $\exp\{gz/c^2\}$ (external mode), and $\exp^{-1}\{Nz\}[\sin nz + n(N - g/c^2)^{-1}\cos nz]$, where $N = \frac{1}{2}(S + g/c^2)$, $n = l\pi/D$, with $l = 1, 2, \ldots$ for the internal modes.

The results of experiments conducted with and without ambient shear flow are compared with those undertaken over a larger horizontal domain. The results are compared during a time interval for which boundary influences are absent from the latter integrations.

A record was kept of the total perturbation energy within the limited domain during the simulations. Fig. 3 shows the time variation of this energy for the three initial states when the ambient flow was assumed to be zero. The dashed and solid lines correspond respectively to the boundary relaxation runs with the limited domain and the results from the integrations with the extended domain.

The total energy remains constant during the initial phase although there are strong interchanges between the various energy forms. Later the energy level drops rapidly as portions of the pulse leave the region through first the east boundary and then the west boundary. A phase lag is observed between the energy-level curves and this is attributable to the energy consumption within the domain in the relaxation boundary regions. This result is corroborated by noting that the horizontal bars in the diagram correspond to the
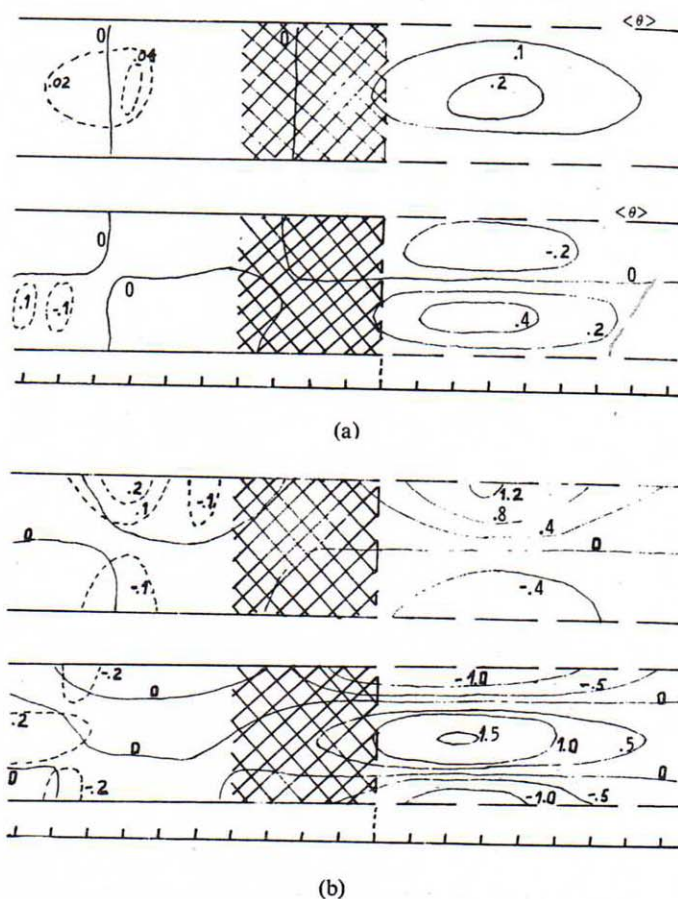
Figure 4.   Instantaneous spatial distribution of (a) the true potential temperature field (solid lines) and error field (dashed lines), and (b) the true u-component velocity field (solid line) and error field (dashed lines). The top and bottom of the diagrams correspond respectively to the first and second internal modes. The interior of the limited domain is to the left of the boundary relaxation region (cross-hatched area).

time for the particular wave mode to traverse the boundary region. It is apparent that the boundary treatment is effective in consuming the outgoing gravity wave energy and that only a comparatively small percentage of this energy is available for spurious reflection to the interior.

The spatial distribution of tne 'true' θ and u fields and the corresponding error fields is shown in Fig. 4 for both the first and second internal modes. The cross-hatched region corresponds to the relaxation region on the east. We note that the pulse, depicted by the solid lines, has almost traversed the boundary of the limited domain. The dashed lines depict the error field, or the difference between the two simulations, in the interior of the limited domain. Weak partial reflection has occurred from the relaxation boundary and the resulting error field has a fine scale structure. Comparable results were obtained with the other external mode simulation.

The time history of the energetics for experiments conducted with moderate shear ($U_z = 3 \times 10^{-3} s^{-1}$) and strong shear ($U_z = 6 \times 10^{-3} s^{-1}$) are shown in Figs. 5 and 6. These results are of some significance since Oliger and Sundstrom (personal communication) indicate that the initial boundary value problem for the non-relaxed, primitive equations is ill-posed. The theoretical difficulties in trying to establish well-posedness arise when an
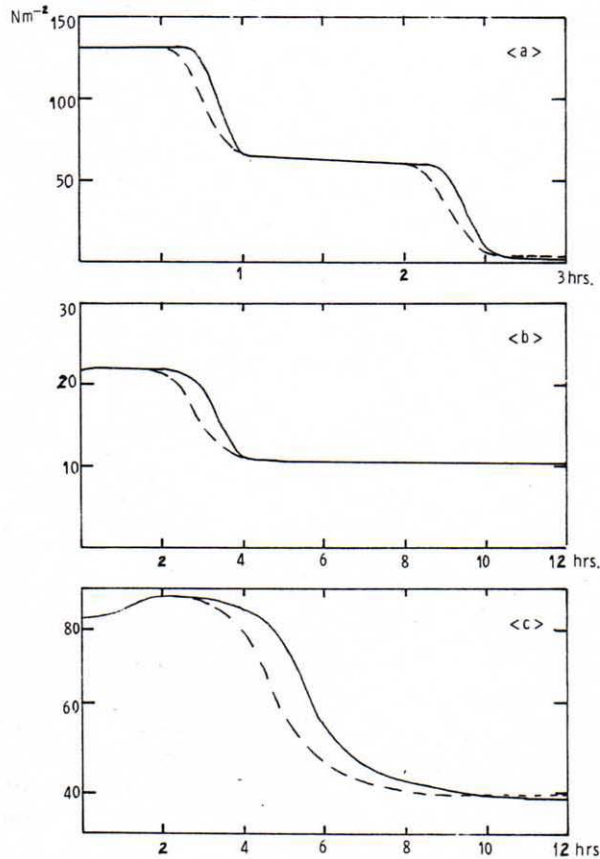
Figure 5.   As for Fig. 3 but with an ambient mean flow shear given by $U_z = 3 \times 10^{-3} \mathrm{s}^{-1}$.

eigenmode of the system has a phase speed intermediate between the maximum and minimum values of the mean flow. Our initial perturbations generate all the permissible modes of our model. Thus these experiments are pertinent to the restrictions placed upon regional models by the mathematical character of the primitive equations. The results suggest that our boundary treatment is satisfactory. The only discomforting features associated with the treatment are minor. Moreover, they occur only with extremely large airflow velocities. We also note that the growth of the total energy in Figs. 5(c) and 6(c) can be shown to be unphysical. It is, however, a truncation effect not associated with the boundary treatment.

These results suggest that, for the model under consideration, the boundary technique provides an adequate treatment of outgoing gravity waves irrespective of their vertical structure and phase speed. Moreover, the method is simple and affords a considerable computational benefit since it circumvents the conventional approach of expanding the variables into the appropriate vertical eigenfunctions at the boundary (Pearson 1974).

(c)   Treatment of quasi-geostrophic flow

The response of the relaxation boundary region to advecting, quasi-geostrophic flow is considered for two forms of limited-domain flow and external boundary data. For the first category (type I) it is assumed that a physically realistic, but quantitatively slightly inaccurate, estimate is available for the time dependent boundary control fields. This
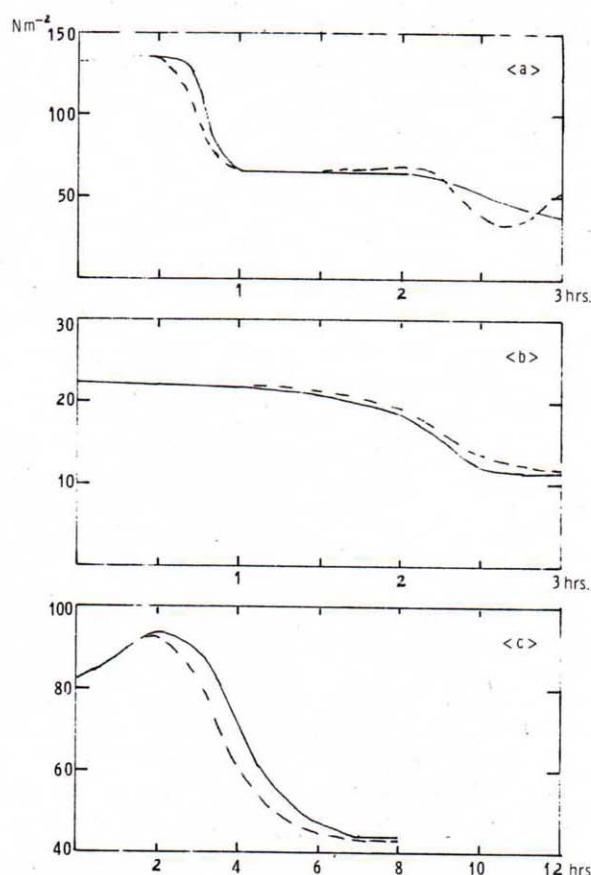
Figure 6.   As for Fig. 3 but with an ambient mean flow shear given by $U_z = 6 \times 10^{-3} \text{s}^{-1}$.

situation resembles a fine-mesh model fed with boundary data derived from a larger domain, coarse-mesh model. For the second category (type II) it is assumed that fine-mesh scale, geostrophic flow is advecting out of the limited region and that no estimate of the boundary data is available *a priori*.

For these experiments, the perturbation geostrophic flow field is given the form

$$
\left.
\begin{aligned}
u &= 0, \\
p &= A \sin(2\pi X/L) \exp\{gz/c^2\}, \\
v &= (2\pi A/fL) \cos(2\pi X/L) \exp\{gz/c^2\},
\end{aligned}
\right\} \tag{12}
$$

with $X = (x - Ut)$, and $t = 0$ at the initial instant.

Here A and L denote respectively the pressure amplitude and the wavelength of the flow, and the flow pattern advects with the constant mean flow U. Initial and boundary conditions for the two flow categories are set out in Table 1.

TABLE 1.   INITIAL AND BOUNDARY CONDITIONS FOR EXPERIMENTS WITH QUASI-GEOSTROPHIC FLOW

Flow type	Pressure amplitude $A(\text{Nm}^{-2})$	Wavelength $L(\text{m})$	Mean flow $U(\text{ms}^{-1})$	Boundary data inflow	outflow
I	$2\cdot5 \times 10^2$	$(61/2)\Delta x$	10	As for Eq. (12) but with U replaced by $(U-1\cdot0)$	
II	$0\cdot833 \times 10^2$	$(61/6)\Delta x$	10	Correct	$\bar{u} \equiv \bar{p} \equiv 0,\ \bar{v}_x \equiv 0$

TABLE 2. INITIAL AND FINAL VALUES OF THE CONSTITUENT FORMS OF PERTURBATION ENERGY PER UNIT VOLUME IN UNITS OF $2 \times 10^{-11} \text{N m}^{-2}$. THE SYMBOLS K.E.($u$), K.E.($v$), E.E., P.E. REFER RESPECTIVELY TO THE KINETIC ENERGY ASSOCIATED WITH THE u AND v-VELOCITY COMPONENTS, THE ELASTIC ENERGY AND THE POTENTIAL ENERGY

Flow type	Simulation time (h)	K.E.(u)	K.E.(v)	E.E.	P.E.
I	0	0·00	3475·0	45·5	0
	8	0·01	3463·0	46·4	0
	16	0·17	3545·0	47·4	0
	24	0·32	3398·0	46·9	0
II	0	0·00	3475·0	5·0	0
	8	0·84	3301·0	7·2	0
	16	0·20	3415·0	9·2	0
	24	1·03	3498·0	10·66	0

One monitor of the technique's performance is the time variation of the constituent forms of the total perturbation energy. Table 2 shows the initial values of these constituents and their values after 8, 16 and 24 hours simulation time. The energy levels should remain constant during the development but again the relaxation boundary acts to consume some of the energy and vitiates a direct comparison. However, it is noteworthy that the potential energy remains zero. This is consonant with the observation that no spurious vertical velocity is generated by the boundary scheme. The kinetic energy of the u component is a measure of the spurious external gravity wave energy generated during the integration and not later consumed in the relaxation boundary region. The maximum grid point error in this component was 0.04 m s^{-1} and 0.12 m s^{-1} at the end of two runs.

The spatial distribution of the true and model derived v-component of the flow fields at mid-level at the end of the integration period is shown in Figs. 7 and 8. These distributions demonstrate the phase lag associated with the difference scheme and the constraint on the
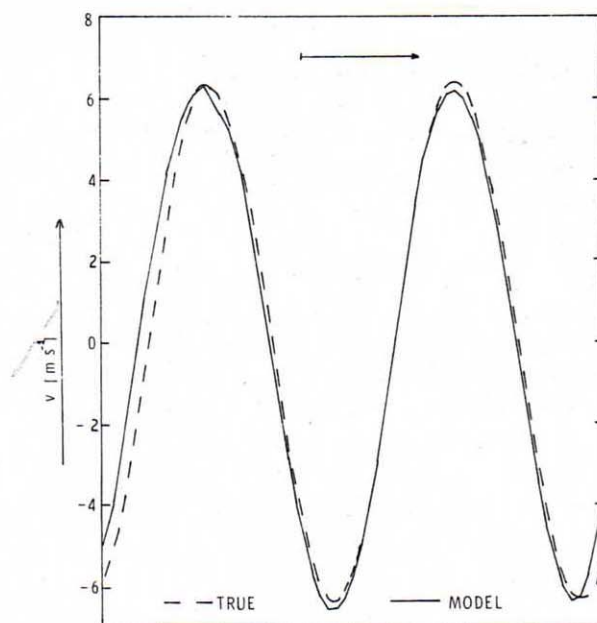

Figure 7. Spatial distribution of the true and model derived v-velocity component at the mid-level after 24 hours of simulation time with a type I flow. Arrow denotes distance moved by pattern in 24 hours, and the vertical boundaries correspond to the model's lateral boundaries.
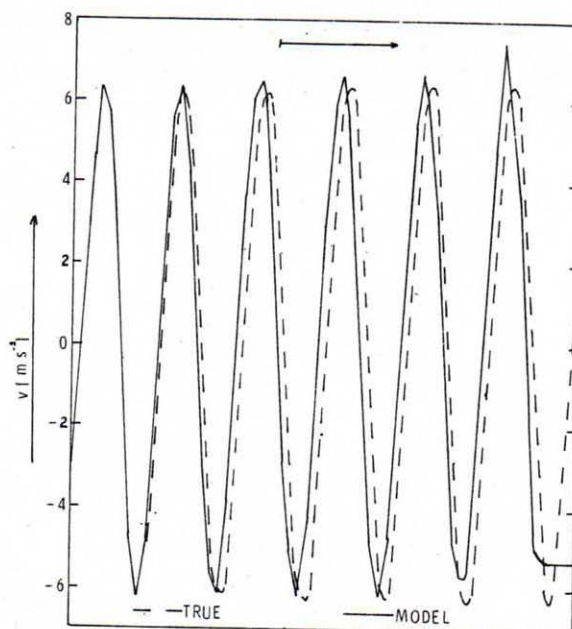
Figure 8. As for Fig. 7 but a type II flow.

horizontal derivative in the boundary region. Apart from these discrepancies, the model-derived distributions bear a close resemblance to the true flow fields, and allows the substantially undistorted transmission of the geostrophic flow into the absorbing boundary region.

An adequate treatment of these two flow categories is essential to the useful application of limited-grid models. The scheme utilized here appears to accomplish this task. Further experiments were carried out varying the values of the parameters A, L and U, and alternative formulations for the error in the boundary conditions for type I flows. These experiments gave qualitatively similar results to those recorded here. They also suggest that the effect of the boundary treatment for type I flows is not crucial provided the boundary data, although overspecified, is sufficiently close to the true flow field. The latter result is helpful in the interpretation of the performance of earlier cavalier treatments of the lateral boundaries of limited-area models.

4. CONCLUDING REMARKS

An expedient treatment has been proposed for the lateral boundaries of a limited-area prediction model. Analytical and numerical results obtained with a linearized, (x, z) multi-level model demonstrated the effectiveness of this computationally efficient technique. A complete extension of the analysis to the three-dimensional, nonlinear, primitive equations is not tractable, and the applicability of the technique to this system of equations is a matter for further experimental examination. We note that it is comparatively simple to implement the technique for a full primitive equation model, and this is illustrated in the appendix.

ACKNOWLEDGMENTS

REFERENCES

Benwell, G. R. R., Gadd, A. J., Keers, J. F., Timpson, M. S. and White, P. W.	1971	The Bushby-Timpson 10-level model on a fine mesh, *Met. Office Scientific Paper No. 32.*
Charney, J. G.	1962	Integration of the primitive and balance equations, *Proc. Int. Symp. Weather Prediction*, Tokyo, pp. 130–252.
Chen, J. H. and Miyakoda, K.	1974	A nested grid computation for the barotropic free surface atmosphere, *Mon. Weath. Rev.*, **102**, pp. 181–190.
Davies, H. C.	1973a	On the lateral boundary conditions for the primitive equations, *J. Atmos. Sci.*, **30**, pp. 147–150.
	1973b	On the initial-boundary value problem of some geophysical fluid flows, *J. Computational Phys.*, **13**, pp. 398–422.
Elvius, T. and Sundström, A.	1973	Computationally efficient schemes and boundary conditions for a fine-mesh barotropic model based on the shallow-water equations, *Tellus*, **25**, pp. 132–156.
Harrison, J. E. J. and Elsberry, R. L.	1972	A method of incorporating nested finite grids in the solution of systems of geophysical equations, *J. Atmos. Sci.*, **29**, pp. 1235–1245.
Kadyshnikov, V. M.	1973	Boundary conditions in the problem of short-term weather forecasting from a baroclinic model of the atmosphere, *Bull. (Izv) Atmospheric and Oceanic Physics*, **9**, pp. 2–4.
Kesel, P. G. and Winninghoff, F. J.	1972	The Fleet Numerical Weather Centre operational primitive equation model, *Mon. Weath. Rev.*, **100**, pp. 300–373.
Oguta, Y. and Charney, J. G.	1962	A numerical model of thermal convection in the atmosphere, *Proc. Int. Symp. Numerical Weather Prediction*, Tokyo, pp. 437–445.
Okamura, Y.	1975	Computational design of a limited-area prediction model, *J. Met. Soc. Japan*, **53**, pp. 175–188.
Pearson, R. A.	1974	Consistent boundary conditions for numerical models of systems that admit dispersive waves, *J. Atmos. Sci.*, **31**, pp. 1481–1489.
Perkey, D. J. and Kreitzberg, C. W.	1975	A time-dependent lateral boundary scheme for limited-area primitive equation models (in preparation).
Phillips, N. A. and Shukla, J.	1973	On the strategy of combining coarse and fine grid meshes in numerical weather prediction, *J. Appl. Met.*, **12**, pp. 763–770.
Price, G. V. and MacPherson, A. K.	1973	A numerical weather forecasting method using cubic splines on a variable mesh, *Ibid.*, **12**, pp. 1102–1113.
Williamson, D. L. and Browning, G. L.	1974	Formulation of the lateral boundary conditions for the NCAR limited-area model, *Ibid.*, **13**, pp. 8–16.

APPENDIX

A formulation of the boundary treatment for the pressure coordinate system

An appropriate extension of the lateral boundary layer formulation to three space dimensions is illustrated here for the 'pressure coordinate' form of the primitive equations. The velocity, continuity and thermodynamic equations take the form,

$$\mathbf{v}_t + (\mathbf{v} \cdot \nabla)\mathbf{v} + \omega \mathbf{v}_p = -\nabla \phi - K(\mathbf{v} - \tilde{\mathbf{v}}) + \mathbf{F}, \quad (\nabla \cdot \mathbf{v}) + \omega_p = 0,$$

$$(\phi_p)_t + (\mathbf{v} \cdot \nabla)(\phi_p) - p^{-1}\omega(\ln \theta)_p = -(pc_p)^{-1}RQ - K(\phi_p - \tilde{\phi}_p),$$

with the following equation for the surface pressure, p^*,

$$p_t^* + (\mathbf{v} \cdot \nabla)p^* - \omega p^* = -K(p^* - \tilde{p}^*).$$

Here we have adopted the standard nomenclature for the thermodymanic variables, whilst $\mathbf{v}$ and the ∇ operator refer respectively to the horizontal components and derivatives. Again the overbarred variables denote the pre-determined boundary control fields.

The horizontal vector $\mathbf{F}$ takes the form,

$$\mathbf{F} = \left\{ \int_{M^*}^{y} (uK_y)\,dy, \int_{L^*}^{x} (vK_x)\,dx \right\},$$

where (L^*, M^*) denote the coordinates of an interior point away from the boundary region.

In their linearized form these equations satisfy criteria similar to those outlined in the main text. We also note that an implicit formulation of the boundary layer terms is again computationally feasible and efficient.